International Journal of Hydrogen Energy 52 (2024) 454–466

Contents lists available at ScienceDirect

International Journal of Hydrogen Energy

journal homepage: www.elsevier.com/locate/he

Liquefied hydrogen value chain: A detailed techno-economic evaluation for its application in the industrial and mobility sectors

Federica Restelli [a,*], Elvira Spatolisano [a], Laura A. Pellegrini [a], Simone Cattaneo [b], Alberto R. de Angelis [b], Andrea Lainati [b], Ernesto Roccaro [b]

[a] GASP - Group on Advanced Separation Processes & GAS Processing, Dipartimento di Chimica, Materiali e Ingegneria Chimica "G. Natta", Politecnico di Milano, Piazza Leonardo da Vinci 32, 20133 Milano, Italy

[b] Eni S.p.A. Research and Technological Innovation Department, via F. Maritano 26, 20097 San Donato Milanese, Italy

ARTICLE INFO

Keywords:
Green hydrogen
Hydrogen liquefaction
Techno-economic analysis
Harbor-to-harbor transport
Liquefied hydrogen storage
Hydrogen refueling stations

ABSTRACT

Green hydrogen can be efficiently produced in regions rich in renewable sources, far from the European large-production sites, and delivered to the continent for utilization in the industrial and mobility sectors. In this work, the transportation of hydrogen from North Africa to North Italy in its liquefied form is considered. A techno-economic assessment is performed on its value chain, which includes liquefaction, storage, maritime transport, distribution, regasification and compression. The calculated transport cost for the industrial application (delivery to a hydrogen valley) ranges from 6.14 to 9.16 €/kg, while for the mobility application (delivery to refueling stations) the range is 10.96–17.71 €/kg. In the latter case, the most cost-effective configuration involves the distribution of liquefied hydrogen and regasification at the refueling stations. The liquefaction process is the cost driver of the value chain in all the investigated cases, suggesting the importance of its optimization to minimize the overall transport cost.

1. Introduction

The exploitation of renewable energy sources (RES) is considered one of the key measures to decarbonize the European economy. The intermittent nature of RES, such as wind and solar power, necessitates efficient energy storage solutions. Hydrogen (H_2) is gaining attention as an energy vector since its production by water electrolysis driven by renewable electricity and its utilization do not involve greenhouse gas emissions. Therefore, it is seen as a potential solution for decarbonizing various sectors, including transportation, industry, and power generation.

One of the critical challenges in realizing the full potential of green hydrogen lies in establishing a robust transportation infrastructure that enables the movement of this clean energy vector across continents, facilitating its utilization in regions with high energy demand, but limited local production capacity. Africa, endowed with vast renewable energy resources, stands as a promising location for large-scale green H_2 production. The continent's abundant and relatively untapped renewable energy potential presents an opportunity to not only generate clean energy for domestic use, but also to export excess energy stored within the hydrogen molecule to energy-demanding regions, such as Europe.

However, transporting gaseous H_2 over long distances presents technical challenges related to its low volumetric density. The liquefaction of hydrogen enables a significant increase in hydrogen density (by approximately 800 times compared to gaseous hydrogen at ambient temperature and pressure) for more efficient storage and transportation. Assessing the economic feasibility of the liquefied hydrogen (LH_2) value chain is essential to determine its viability as an energy carrier.

The LH_2 value chain (Fig. 1) includes liquefaction, storage, transportation, distribution and regasification. Hydrogen produced by RES-driven water electrolysis is the input to the value chain, while its final utilization is envisaged in the industrial, power generation and mobility sectors.

Other commonly investigated carriers for long-distance H_2 transport are liquefied ammonia (LNH_3) [1], methanol [2] and liquid organic hydrogen carriers (LOHC), such as toluene, dibenzyltoluene [3] and N-ethylcarbazole [4]. They all involve an exothermic reaction to chemically bond hydrogen to another compound and an endothermic reaction to release the stored hydrogen. Techno-economic assessments of the liquefied hydrogen value chain are commonly found in the literature, particularly when compared with the use of alternative carriers.

* *Corresponding author.*
E-mail address: federica.restelli@polimi.it (F. Restelli).

https://doi.org/10.1016/j.ijhydene.2023.10.107
Received 14 June 2023; Received in revised form 29 August 2023; Accepted 9 October 2023
Available online 31 October 2023

Abbreviations:

BOG	Boil-Off Gas
CAPEX	CAPital EXpenditures
CCS	Carbon Capture and Sequestration
CEPCI	Chemical Engineering Plant Cost Index
CW	Cooling Water
DMC	Direct Manufacturing Costs
FMC	Fixed Manufacturing Costs
GE	General Expenses
HRS	Hydrogen Refueling Stations
IEA	International Energy Agency
IFO	Intermediate Fuel Oil
IRENA	International Renewable Energy Agency
J-B	Joule-Brayton
J-T	Joule-Thomson
LCoHT	Levelized Cost of Hydrogen Transport
LH_2	Liquefied Hydrogen
LNG	Liquefied Natural Gas
LNH_3	Liquefied Ammonia
LOHCs	Liquid Organic Hydrogen Carriers
OPEX	OPerating EXpenditures
PV	PhotoVoltaic
RES	Renewable Energy Sources
RW	Refrigerated Water
WACC	Weighted Average Cost of Capital

Table 1 provides a summary of the existing literature on this subject.

Referring to the reviewed literature, a wide range of hydrogen production capacities is assumed in the different works, the choice depending on the primary energy source, RES or fossil-based, and on the available area to install the renewable power plant. For example the H_2 production capacity of 44 t/d assumed by Gallardo et al. [9] requires 400 MW of installed photovoltaic (PV) power. Considering as rule of thumb a specific area of 10 m^2 per installed kW [22], this results in a total area occupied by the PV power plant of about 4 km^2. The assumed export terminals are locations with high availability of renewable sources, high solar radiation and/or strong wind speed, such as North Africa, Middle East, Australia, Latin America and North Sea, or, in some cases, of natural gas from which hydrogen is obtained via reforming reaction with or without subsequently carbon capture and sequestration (CCS), such as Qatar, Norway and Canada. Japan is selected as the import terminal in many studies [5,8–10,13,16–19] because of the large H_2 demand determined by the Japanese commitment to achieve net-zero greenhouse gas emissions by 2050 [23]. Central Europe is also commonly chosen as importing region because of its limited domestic production from RES and its efforts in transitioning to a low-carbon economy [17].

In summary, there is currently significant ongoing research activity concerning the techno-economic analysis of hydrogen transportation in its liquefied form. However, to the authors' knowledge, none of the existing literature works involves simulation of the cost-driving processes, hydrogen liquefaction and regasification, in order to estimate their capital and operating expenditures from the resulting material and energy balances. Furthermore, no techno-economic assessments are reported in the literature which differentiate among the possible applications of the delivered hydrogen. The novelty of the present article lies in addressing these gaps in the existing literature. The aim of this work is to perform a techno-economic evaluation of hydrogen transportation in its liquid state from North Africa to North Italy. The cost driver of the LH_2 value chain is certainly the liquefaction process. Therefore, special attention is paid to the selection of the configuration for this process. Three different liquefaction processes are simulated using the commercial software Aspen Plus® V.11 [24]: a liquid nitrogen precooled Claude cycle (currently adopted technology), a mixed refrigerant precooled Claude cycle and a mixed refrigerant cascade process. These simulations yield material and energy balances, which are then used to assess the capital and operating expenditures of the three configurations, with the aim to identify which one is the most cost-effective for the examined case study. Two alternatives for the utilization of the delivered H_2 are explored: end use in the industrial sector, with hydrogen being transported to a H_2 valley, and application in the mobility sector, necessitating the transport of hydrogen to a number of refueling stations. For the latter, an analysis is performed to identify at which location, port or refueling stations, is better to perform the reconversion to gaseous hydrogen.

2. Basis of design

A feasibility study is carried out on the transportation of green hydrogen from a theoretical renewable electricity production plant situated in North Africa to a theoretical utilization site located inland 100 km from a Mediterranean port, covering a harbor-to-harbor distance of approximately 2500 km. Green hydrogen is supposed to be produced with a constant flow rate of 20000 Nm^3/h using an alkaline electrolyzer, hence it is at 20 bar and 25 °C. The hydrogen is transported in its liquid state at −252 °C and pressure slightly above the atmospheric one. Two potential destinations for the delivered hydrogen are investigated: firstly, a H_2 valley, operating at 30 bar, wherein all the hydrogen is directed for industrial end use (with a required H_2 purity of 99.9 mol%), and, secondly, H_2 Refueling Stations (HRS), each demanding 500 kg-H_2/d, to serve the mobility sector (with a required H_2 purity of 99.97 mol%, as per ISO 14687:2019). The H_2 pressure at the HRS is 900 bar, required to fill the car tanks, typically at 700 bar. The value chain consists of liquefaction, storage at the loading port, sea transport, storage at the unloading port, distribution, storage at the end user/users, regasification and, if required, compression. Green H_2 production and final utilization are excluded from the system's boundaries. Two possible configurations are envisaged for H_2 delivery to refueling stations: decentralized regasification at the end users' locations, involving the upstream distribution of liquefied H_2, and centralized regasification at the unloading port, entailing the downstream distribution of gaseous H_2, suitably compressed for transportation via trucks.

Because of the substantial increase in inflation that affected the year 2022, distinct scenarios are examined: a "present" scenario that

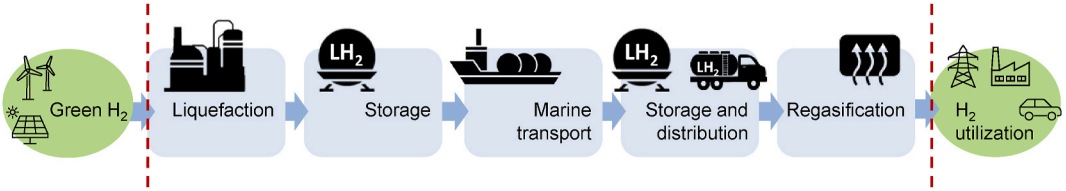

Fig. 1. Liquefied hydrogen value chain.

considers the current expenses for utilities, and a "future" scenario that takes into account the forecasted reduction in costs in the next four years.

3. Methodology of techno-economic evaluation

To evaluate the hydrogen transport cost at every stage of the value chain, as described in Section 2, for the scenarios under investigation, the Levelized Cost of Hydrogen Transport (*LCoHT*) [25] is calculated according to Eq. (1):

$$LCoHT = \frac{\sum_{t=0}^{N-1} \frac{CAPEX_t + OPEX_t}{(1+WACC)^t}}{\sum_{t=0}^{N-1} \frac{F_{H_2,out}}{(1+WACC)^t}} \quad (1)$$

where $F_{H2,out}$ is the mass flow rate of hydrogen delivered yearly, t is the year (being $t = 0$ the base year and *N-1* the final year), $CAPEX_t$ and $OPEX_t$ are the capital and operating expenditures, respectively, at time t and *WACC* is the weighted average cost of capital. The assumptions for the economic assessment are reported in Table 2.

Table 2
Assumptions for the economic assessment.

Item	Value
Base year ($t = 0$)	2022
WACC	5 %
Project lifetime	25 y
Plant availability (H_{eq})	8000 h/y
Construction period	3 y (*CAPEX* subdivision: 40 %, 30 %, 30 %)
Decommissioning cost	5 % *CAPEX* [26]
Exchange rate (2022)	0.951 €/US-$ [27]

3.1. Cost-driving processes

The economic evaluation of the cost drivers of the value chain, conversion and reconversion processes, is carried out in accordance with the Turton methodology [28]. The approach employed is intended for a preliminary feasibility study and provides a rough estimation of the plant expenses with an accuracy of ±30 %. Using the Guthrie method [29], the capital expenditures (*CAPEX*) of the plant are determined by computing the purchased base cost $C^0_{p,i}$ for each piece of equipment using Eq. (2):

$$\log_{10}\left(C^0_{p,i}(2001)\right) = K_{1,i} + K_{2,i}\log_{10}(A_i) + K_{3,i}[\log_{10}(A_i)]^2 \quad (2)$$

Table 1
List of literature regarding techno-economic assessment of the liquefied hydrogen value chain.

Reference	H_2 capacity [t/d]	H_2 source	Export terminal	Import terminal	Other carriers analyzed
Okunlola et al., 2022 [5]	607	natural gas reforming + CCS	Canada (Alberta)	Japan, China, South Korea, Germany, UK	LNH_3
Chodorowska and Farhadi, 2021 [6]	500	natural gas reforming + CCS	Qatar	United Kingdom	LNG, LNH_3, LOHC (toluene)
Roland Berger, 2021 [7]	20 200	H_2O electrolysis powered by RES	Middle East (Arabian Gulf)	Europe	LNH_3, LOHC (benzyltoluene)
Raab et al., 2021 [8]	677	H_2O electrolysis powered by RES	Australia (Melbourne)	Japan (Tokyo)	LOHC (toluene and dibenzyltoluene)
Gallardo et al., 2021 [9]	44	H_2O electrolysis powered by RES	Chile (Antofagasta)	Japan (Osaka)	LNH_3
Song et al., 2021 [10]	9000 60000	H_2O electrolysis powered by RES	China	Japan	LNH_3, LOHC (toluene)
Niermann et al., 2021 [11]	500	H_2O electrolysis powered by RES	Algeria (Algiers)	Germany (Hamburg)	methanol, LOHC (toluene, dibenzyltoluene, N-ethylcarbazole)
Hong et al., 2021 [12]	1000	natural gas reforming + CCS and H_2O electrolysis powered by RES	Australia, Malaysia, Indonesia	Singapore	LNH_3, LOHC (toluene)
Ishimoto et al., 2020 [13]	500	90 % natural gas reforming + CCS 10 % H_2O electrolysis powered by RES	Norway	Japan (Tokyo) Europe (Rotterdam)	LNH_3
Hank et al., 2020 [14]	130	H_2O electrolysis powered by RES	Morocco	Germany	LNH_3, methanol, LNG, LOHC (dibenzyltoluene)
Hydrogen Import Coalition, 2020 [15]	1800	H_2O electrolysis powered by RES	Morocco	Belgium	LNH_3, methanol, LNG, LOHC (dibenzyltoluene)
Wijayanta et al., 2019 [16]	900	coal gasification and H_2O electrolysis powered by RES	Australia (Victoria)	Japan (Tokyo)	LNH_3, LOHC (toluene)
IEA, 2019 [17]	700	natural gas reforming + CCS and H_2O electrolysis powered by RES	Australia North Africa	Japan Europe	LNH_3, LOHC (toluene)
Kamiya et al., 2015 [18]	770	coal gasification + CCS	Australia	Japan	–
Teichmann et al., 2012 [4]	3000	H_2O electrolysis powered by RES	North Africa	Europe	LOHC (N-ethylcarbazole)
Watanabe et al., 2010 [19]	16400	H_2O electrolysis powered by RES	Patagonia	Japan	–
Stiller et al., 2008 [20]	–	H_2O electrolysis powered by RES	Norway	Germany	–
Wietschel and Hasenauer, 2007 [21]	900	H_2O electrolysis powered by RES	Iceland Norway Morocco Algeria	UK Denmark Spain Italy	–

where the constants $K_{1,i}$, $K_{2,i}$ and $K_{3,i}$ are available in Ref. [28] and allow to evaluate the cost of the equipment referred to the year 2001. A_i is the capacity or size parameter, specific to the type of equipment. In order to get a current estimate, it is necessary to update this cost considering economic inflation. This can be accomplished by using the following expression:

$$C_2 = C_1\left(\frac{I_2}{I_1}\right) \tag{3}$$

where C represents the purchase cost, I stands for a cost index and the subscripts denote different time points. In this analysis, the chosen cost index is the Chemical Engineering Plant Cost Index (*CEPCI*), with $CEPCI_{2001} = 397$ and $CEPCI_{2022} = 816.5$.

To consider the effect of construction material and operating pressure on the equipment cost, the concept of bare module cost ($C_{BM,i}$) is introduced and computed using the following equation:

$$C_{BM,i} = C^0_{p,i}F_{BM,i} = C^0_{p,i}\left(B_{1,i} + B_{2,i}F_{M,i}F_{P,i}\right) \tag{4}$$

where $F_{BM,i}$ is the bare module factor and is determined by the parameters $F_{M,i}$ (material factor), related to the construction material, and $F_{P,i}$ (pressure factor), which accounts for the operating pressure of the equipment. The constants $B_{1,i}$ and $B_{2,i}$, specific to each equipment type i, can be found in Ref. [28].

The bare module cost for equipment in carbon steel and operating at atmospheric pressure ($C^0_{BM,i}$), as well as the corresponding bare module factor ($F^0_{BM,i}$), are obtained by setting $F_M = F_P = 1$.

Using Eq. (5), the total module cost (C_{TM}) is computed increasing by 18 % the bare module cost of the equipment, to take into account fees and contingency costs. The *CAPEX*, as in Eq. (6), take into account the cost for auxiliary buildings, site development, off-sites and utilities (grassroots cost) by appropriately increasing the total module cost.

$$C_{TM} = 1.18\sum_{i=1}^{n} C_{BM,i} \tag{5}$$

$$CAPEX = C_{TM} + 0.5\sum_{i=1}^{n} C^0_{BM,}i \tag{6}$$

The operating expenditures (*OPEX*) of the plant are calculated by adding up various cost components belonging to three major cost categories: Direct Manufacturing Costs (*DMC*), which are expenses that change according to production rate, Fixed Manufacturing Costs (*FMC*), which remain constant irrespective of changes in production rate and include property taxes, insurance, and plant overhead expenses, and General Expenses (*GE*), which are expenses that rarely change according to production rate and include sales, management, financing and research functions.

To evaluate the *OPEX*, it is necessary to have knowledge of, or at least the ability to estimate, the following costs: *CAPEX*, cost of utilities (C_{UT}), cost of operating labor (C_{OL}), cost of raw materials (C_{RM}) and cost of waste treatment (C_{WT}). Table 4 reports the factors for estimating the operating cost.

C_{UT} involves the costs associated with the consumption of electricity, cooling water (CW) and refrigerated water (RW). Table 3 reports the specific utility costs utilized in this work for the "present" and "future" scenarios. Utility consumption is determined from the energy balances obtained through process simulation.

Table 3
Utility costs for the "present" and "future" scenarios.

Utility	Units	"present"	"future"
Electricity	€/MWh	500	220
CW (30 °C)	€/GJ	0.3583	0.3583
RW (15 °C)	€/GJ	32.3408	14.4768

Table 4
Estimation of OPEX in accordance with the Turton methodology [28].

Operating cost category	Calculated as
Direct Manufacturing Costs (*DMC*)	$C_{UT} + 1.33{\cdot}C_{OL}{+}0.069{\cdot}CAPEX{+}0.03{\cdot}OPEX$
Utilities (C_{UT}) Operating labor (C_{OL}) Raw Materials (C_{RM}) Waste treatment (C_{WT}) Maintenance and repairs Direct supervisory and clerical labor Operating supplies Patents and royalties Laboratory charges	
Fixed Manufacturing Costs (*FCM*)	$0.708{\cdot}C_{OL} + 0.068{\cdot}CAPEX$
Plant overhead costs Local taxes and insurance	
General Expenses (*GE*)	$0.177{\cdot}C_{OL} + 0.009{\cdot}CAPEX + 0.21{\cdot}OPEX$
Distribution and selling costs Administration costs Contingency Research and development	
***OPEX* (*DMC* + *FMC* + *GE*)**	$C_{UT} + 2.215{\cdot}C_{OL} + 0.24{\cdot}OPEX{+}0.146{\cdot}CAPEX$

The expenses incurred for personnel required for plant operations (C_{OL} [M€/y] in Eq. (7)) are determined by the number of operators required per shift, N_{OL}, and the average annual wage of an operator, C_{labor}, which is assumed to be 40000 €/y. A single operator typically works for five 8-h shifts a week, for a total of 45 weeks in a year. N_{OL} is calculated according to Eq. (8) [28] for full-capacity plants at the ports and H_2 valley, while it is set equal to 1 for small-scale plants at the HRS.

$$C_{\text{OL}} = C_{\text{labor}}{\cdot}N_{\text{OL}}{\cdot}\frac{H_{\text{eq}}}{45{\cdot}5{\cdot}8}{\cdot}10^{-6} \tag{7}$$

$$N_{OL} = \text{round up}\left[(6.29 + 0.23{\cdot}N_u)^{0.5}\right] \tag{8}$$

In Eq. (8) N_u is the number of process units (excluding valves and pumps).

C_{RM} accounts for the expenses associated with the chemical feedstocks needed by the process. They are supposed to be negligible in this analysis, although rigorously they take into account the cost of the refrigerants flowing in closed cycles and their make-up. The cost of waste treatment (C_{WT}) is considered null in the present analysis.

3.2. Maritime transport

Regarding the maritime transportation of the LH_2, the *CAPEX* associated with the purchase of the vessel and the *OPEX* associated with the labor, fuel and CO_2 emissions costs are taken into account. The expenses related to maintenance and insurance are neglected.

It is assumed to purchase a single vessel, whose capacity is computed considering the quantity of LH_2 produced and stored at the port during the period when the vessel is not present at the loading port ($t_{\text{prod. to store}}$), which is calculated as follows:

$$t_{\text{prod. to store}} = t_{\text{round trip}} + t_{\text{loading and unloading}} + t_{\text{safety margin}} \tag{9}$$

where $t_{\text{round trip}}$ is the time required for the round trip, $t_{\text{loading and unloading}}$ is the time needed for the loading and unloading operations, assumed equal to 1 day, and $t_{\text{safety margin}}$ is the safety margin time to manage possible delays, assumed equal to 2 days. Assuming a ship speed of 16 knots (approximately 30 km/h), the $t_{\text{prod. to store}}$ is equal to 10 days.

The vessel's gross capacity (V_{vessel} [m^3] in Eq. (10)) is computed taking into account that it is possible to fill up to a maximum of 98 % of the volume due to safety considerations and that a residue volume of 4 % must remain inside the vessel for cooling purposes, as for the LNG tanks

[30].

$$V_{\text{vessel}} = \frac{F_{H_2} \cdot 24 \cdot t_{\text{prod. to store}}}{\rho_{LH_2} \cdot (0.98 - 0.04)} \quad (10)$$

In Eq. (10) F_{H2} [kg/h] is the hydrogen flow rate and ρ_{LH2} is the volumetric density of LH_2, equal to 70 kg/m^3.

Table 5 reports the investment costs of the LNG vessels are retrieved from the work by Fikri et al. [31]. They are adjusted for inflation to the year 2022 using the *CEPCI* and then interpolated using a power law to obtain the *CAPEX* of the vessel ($CAPEX_{\text{vessel}}$ [M€] in Eq. (11)) as a function of its gross capacity.

$$CAPEX_{\text{vessel}} = 0.7316 \cdot V_{\text{vessel}}^{0.496} \quad (11)$$

To calculate the operating costs related to the labor ($OPEX_{\text{labor}}$ [M€/y] in Eq. (12)), a crew size (*Crew* in Eq. (12)) of 16 people, as indicated in the technical data sheet of a LNG vessel with almost the same capacity as that of the vessel considered in this study [32], is taken into account. It is assumed that two complete crews alternate in one year and that each operator has an annual wage (C_{labor} in Eq. (12)) of 52000 €/y.

$$OPEX_{\text{labor}} = C_{\text{labor}} \cdot Crew \cdot 2 \cdot 10^{-6} \quad (12)$$

It is assumed that the vessel is powered by a conventional fuel engine, such as Intermediate Fuel Oil (IFO 380). The cost of this fuel (C_{fuel} in Eq. (13)) is supposed equal to 580 €/t in the "present" scenario and 450 €/t in the "future" scenario. To determine fuel consumption ($Cons_{\text{fuel}}$ in Eq. (13)) an engine power of 3000 kW, as indicated in the technical data sheet previously considered [32], and a specific fuel consumption of 0.1587 kg/kWh [5] are adopted. Therefore, the operating costs related to fuel consumption ($OPEX_{\text{fuel}}$ [M€/y] in Eq. (13)) are computed as:

$$OPEX_{\text{fuel}} = C_{\text{fuel}} \cdot Cons_{\text{fuel}} \cdot \frac{t_{\text{round trip}}}{t_{\text{prod. to store}}} \cdot \frac{H_{\text{eq}}}{24} \cdot 10^{-6} \quad (13)$$

The operating costs related to CO_2 emissions ($OPEX_{CO2}$ [M€/y] in Eq. (14)) are computed based on a CO_2 emissions cost (C_{CO2} in Eq. (14)) of 90 €/t in the "present" scenario and 105 €/t in the "future" scenario. Moreover, specific CO_2 emissions per fuel volume (e_{fuel} in Eq. (15)) of 11.24 $kg_{CO2}/gallon_{IFO\ 380}$ [33] are considered.

$$OPEX_{CO_2} = E_{\text{fuel}} \cdot C_{CO_2} \cdot \frac{t_{\text{round trip}}}{t_{\text{prod. to store}}} \cdot \frac{H_{\text{eq}}}{24} \cdot 10^{-6} \quad (14)$$

In Eq. (15) E_{fuel} [t/d] is the CO_2 emissions rate, computed as:

$$E_{\text{fuel}} = \frac{Cons_{\text{fuel}} \cdot e_{\text{fuel}} \cdot 264.2[\text{gallon/m}^3]}{\rho_{\text{IFO 380}}} \quad (15)$$

where $\rho_{\text{IFO 380}}$ represents the volumetric density of IFO 380, which is 990 kg/m^3.

During maritime transport, a quantity of LH_2 amounting to 0.2%/d is lost due to the boil-off phenomenon. Although the hydrogen gas can be harnessed for onboard heating or power generation, in this analysis it is assumed not to recover its value and to send it to a flare.

Table 5
Vessel's gross capacity (V_{vessel} [m^3]), reference year and *CAPEX* [M$], taken from Fikri et al. [31].

V_{vessel} [m^3]	Reference year	Reference *CAPEX* [M$]
6000	2015	50
7500	2018	37
12000	2014	50
28000	2018	80
30000	2014	105

3.3. Storage

Liquefied hydrogen is stored inside spherical tanks, to minimize the area/volume ratio, at about −252 °C and a pressure slightly above the ambient one (1.3 bar). These tanks are equipped with vacuum perlite insulation to reduce the heat transfer from the ambient and, hence, minimize the losses due to the boil-off phenomenon.

Regarding the storage of the LH_2, only the *CAPEX* associated with the purchase of the storage tank are taken into account, while the *OPEX* are neglected. The losses due to boil off are assumed to be negligible, as it is possible to reliquefy the boil-off gas at the loading port and to compress and warm it at the site where regasification occurs.

A power law for estimating the investment costs associated with the tank ($CAPEX_{\text{tank}}$ in Eq. (16)) is obtained by interpolating the cost data reported in Ref. [34], after being adjusted for inflation to 2022 using the *CEPCI* and multiplied by a factor of 1.3 to account for the installation cost.

$$CAPEX_{\text{tank}} = 0.057 \cdot V_{\text{tank}}^{0.6891} \quad (16)$$

For each terminal operating at full capacity (loading and unloading ports, and H_2 valley), it is assumed to purchase a single tank, whose gross capacity (V_{tank} [m^3] in Eq. (17)) is computed considering the storage of the volume transported by the vessel increased by 10 % as a safety margin to manage possible delays.

$$V_{\text{tank}} = (1 + 0.1) \cdot V_{\text{vessel}} \quad (17)$$

Regarding the case of decentralized regasification at the HRS, it is assumed that a small LH_2 storage tank, with a capacity of 9 m^3, is purchased for each refueling station. The *CAPEX* for this tank are estimated to be 0.088 M€ (value obtained from Ref. [34], adjusted for inflation to 2022).

3.4. Distribution

Regarding road distribution, the analysis takes into account the *CAPEX* associated with the purchase of the trucks and the *OPEX* associated with the labor, fuel and CO_2 emissions costs. The expenses related to maintenance and insurance are neglected.

The calculation of the required number of trucks to purchase (n_{trucks} in Eq. (18)) takes into account that each truck completes two round trips per day:

$$n_{\text{trucks}} = \text{round up}\left(\frac{M_{\text{unloaded from the vessel}}}{M_{\text{truck}} \cdot t_{\text{prod. to store}} \cdot 2}\right) \quad (18)$$

where M_{truck} [kg] represents the net capacity of a single truck and $M_{\text{unloaded from the vessel}}$ [kg] stands for the mass of LH_2 unloaded from the vessel at the destination port. The computation of $M_{\text{unloaded from the vessel}}$ considers that a portion of the initially loaded volume is lost due to the boil-off phenomenon, with a rate (r_{BOG} in Eq. (19)) of 0.2%/d:

$$M_{\text{unloaded from the vessel}} = F_{H_2} \cdot t_{\text{prod. to store}} \cdot (1 - r_{BOG})^{t_{\text{round trip}}/2} \quad (19)$$

Distribution can occur either upstream or downstream of the regasification process. In the former case, liquefied hydrogen would be distributed using trucks, designed to operate at −252 °C and 1.3 bar, and the regasification process would be performed at the destination site. In the latter case, gaseous hydrogen would be distributed using trucks, stored in appropriate cylindrical tanks (tube trailers) designed to operate at ambient temperature and 250 bar. Hydrogen gas is discharged from the tube trailers by reducing the pressure to 15 bar.

Trucks consist of two main components: the tractor unit, housing the driver's cab, and the trailer unit. The same tractor unit is utilized for both liquefied and compressed hydrogen trucks, having an investment cost of 0.29 M€ (value obtained from Ref. [35], adjusted for inflation to 2022). On the contrary, the type of trailer and its maximum capacity depend on its cargo. For liquefied H_2, a trailer with a net capacity M_{truck}

of 4000 kg is selected, with *CAPEX* of 1.19 M€ (value retrieved from Ref. [36], adjusted for inflation to 2022), while a compressed gaseous H_2 trailer with a M_{truck} of 500 kg and *CAPEX* of 0.57 M€ (value retrieved from Ref. [36], adjusted for inflation to 2022) is adopted. The trucks' lifetime is assumed to be 12 years.

The labor operating costs ($OPEX_{labor}$ [M€/y] in Eq. (20)) are computed with the assumption that the number of drivers per shift matches the number of trucks. It is further considered that each individual operator receives an annual wage (C_{labor} in Eq. (20)) of 40000 €/y and operates for 45 weeks annually, encompassing five 8-h shifts per week.

$$OPEX_{labor} = C_{labor} \cdot n_{trucks} \cdot \frac{H_{eq}}{45 \cdot 5 \cdot 8} \cdot 10^{-6} \quad (20)$$

It is assumed that trucks run on diesel and have a fuel consumption rate of 35 L/100 km [37]. Accordingly, the operating costs associated with fuel consumption ($OPEX_{fuel}$ [M€/y] in Eq. (21)) are determined as follows:

$$OPEX_{fuel} = C_{fuel} \cdot Cons_{fuel} \cdot d \cdot 2 \cdot \frac{V_{unloaded\ from\ the\ ship}}{V_{truck} \cdot t_{prod.\ to\ store}} \cdot \frac{H_{eq}}{24} \cdot 10^{-6} \quad (21)$$

where d represents the distance between the unloading port and the end user, which is equal to 100 km, and C_{fuel} stands for the cost of diesel, which is assumed to be 1.8155 €/L (average price of diesel in Italy in 2022) for both the "present" and "future" scenarios. The operating costs related to CO_2 emissions are computed by taking into account that diesel fuel has specific CO_2 emissions (e_{fuel} in Eq. (22)) of 10.19 $kg_{CO2}/gallon_{diesel}$ [33].

$$OPEX_{CO_2} = C_{CO_2} \cdot E_{fuel} \cdot d \cdot 2 \cdot \frac{V_{unloaded\ from\ the\ ship}}{V_{truck} \cdot t_{prod.\ to\ store}} \cdot \frac{H_{eq}}{24} \cdot 10^{-6} \quad (22)$$

In Eq. (22) E_{fuel} [t/km] is computed as:

$$E_{fuel} = Cons_{fuel} \cdot e_{fuel} \cdot 264.2 \left[gallon \,/\, m^3 \right] \cdot 10^{-6} \quad (23)$$

4. Simulation of the conversion process

The conversion from gaseous to liquid hydrogen is attained via the liquefaction process. It consists in the cooling of hydrogen to the condition of saturated liquid at the storage tank pressure (1.3 bar) and involves catalytic ortho-para conversion so that equilibrium ortho-para composition is obtained at the end of the process. Several process diagrams are available for hydrogen liquefaction: from the simple liquid nitrogen (LN_2) precooled Claude cycle to the complex mixed-refrigerant (MR) cascade process. Review articles about this topic are present in the literature [38–41].

In the present work, three different process configurations, at increasing efficiency (and complexity), are considered: a LN_2 precooled Claude cycle, a MR precooled Claude cycle and a MR cascade process. They are simulated with the aim to compare their performances and assess which one is the most cost-effective for the given basis of design. This configuration shows the best trade-off between *OPEX*, related to the utilities consumption and, hence, decreasing at increasing efficiency, and *CAPEX*, related to the process complexity, generally increasing with the efficiency.

For comparison purposes, common assumptions are made for all the simulated processes. The ortho-para catalytic conversion, which allows to reach the equilibrium at the end of the liquefaction process to avoid excessive boil off during storage, is performed along the heat exchangers' tubes where a suitable catalyst is packed on the processed hydrogen side. For the sake of simplicity, pressure drops inside the heat exchangers are neglected. All the pieces of equipment are embedded in coldboxes to limit the heat exchange with the surroundings. The simulations are carried out using the Aspen Plus® V.11 [24] commercial software, selecting the Peng-Robinson thermodynamic package with the modifications described by Restelli et al. [42] to represent the behavior of equilibrium-hydrogen, the temperature-dependent equilibrium mixture of ortho- and para-hydrogen. The choice of this Equation of State (EoS) is justified by its combined accuracy and ease of implementation within the simulator. Although more accurate EoSs exist, such as the one proposed by Leachman et al. [43], with the modification proposed by Valenti et al. [44] to describe the equilibrium-H_2, and the one proposed by Balasubramanian et al. [45] to describe ortho- and para-H_2 and their mixtures, the chosen thermodynamic model strikes a balance between accuracy and practicality.

4.1. Liquid nitrogen precooled Claude cycle

As an example of the LN_2 precooled Claude cycle process scheme, the one described by Crawford [46] is taken with minor modifications and is depicted in Fig. 2.

Considering the scheme in Fig. 2, the inlet hydrogen stream GH2 is mixed with the recycle streams 14 and 18 to form stream 1, which is cooled to 25 °C using service water and then compressed in an intercooled two-stage compressor C-1. The outlet stream 3 from C-1 is at 103 bar and 25 °C and is cooled in multi-pass heat exchangers HX-1 and HX-2 by warming the recycle gaseous hydrogen streams at low and intermediate pressure. The heat exchanger HX-1 includes a cold stream 19 of liquid nitrogen boiling at a pressure of 1.1 bar. Both heat exchangers are characterized by a minimum temperature approach of 2 °C. The process stream is cooled to −208 °C (stream 4) in HX-1 and to −232 °C (stream 5) in HX-2 before reducing its pressure in Joule-Thomson (J-T) valve VLV-1. Stream 6 at the outlet of VLV-1 is at 5.5 bar and −246 °C. Under these conditions, the stream is biphasic and is separated in flash vessel V-1. The vapor is recycled back to cool the process stream in HX-1 and HX-2. The liquid is passed through the process-process heat exchanger HX-3, which is characterized by a minimum temperature approach of 1 °C and is further cooled passing through the J-T valve VLV-2, reaching the storage pressure of 1.3 bar. At the outlet of VLV-2 the process stream is at −252 °C and is sent to flash vessel V-2 in order to separate its vapor and liquid phases. The vapor from the top of V-2 is recycled back, passing through the cold side of the heat exchangers HX-3, HX-2 and HX-1. The liquid from the bottom of V-2 leaves the process to be stored in an insulated tank at 1.3 bar pressure. The energy balance of the process is presented in Table 6 and Table 7, detailing the cooling duties and electric power consumptions, respectively.

4.2. Mixed-refrigerant precooled Claude cycle

To simulate the MR precooled Claude Cycle reference is made to the work by Cardella et al. [47]. The process scheme is depicted in Fig. 3.

With reference to the process diagram in Fig. 3, the hydrogen feed GH2 is precooled down to −173 °C in a multi-pass heat exchanger HX-1, where a mixture of 14 mol% N_2, 30 mol% CH_4, 31 mol% C_2H_6 e 25 mol% i-C_4H_{10} is used as refrigerant within a J-T cycle. Subsequently, the processed hydrogen is cooled to −250 °C in a series of heat exchangers, HX-2, HX-3, HX-4 and HX-5, thanks to a H_2 Claude cycle.

The precooling mixture (stream 11) is compressed to 50 bar in two compressor stages (C-1 and C-2) with intercooling to 40 °C. Downstream of the C-2 aftercooler, E−2, the high-pressure stream 19 is separated into its vapor (stream 20) and liquid (stream 24) phases. These streams are precooled in HX-1 and expanded to 2.9 bar in J-T valves, VLV-2 and VLV-3, to reach two different precooling temperatures −177 °C and −112 °C, respectively. The low-pressure streams 23 and 27 act as cold fluids in HX-1 and are mixed at its outlet.

The design of the Claude cycle has been optimized by Cardella et al. [47] to reduce the temperature differences in the heat exchangers. The J-T part of the Claude cycle is designed with a turbine TE-4 upstream of the final J-T valve VLV-4, which performs the expansion to 1.4 bar. The Brayton part of the Claude cycle is designed with two turbines TE-2 and TE-3 expanding to the intermediate pressure of 8.3 bar, to remove heat from the processed hydrogen stream at two different temperature levels:

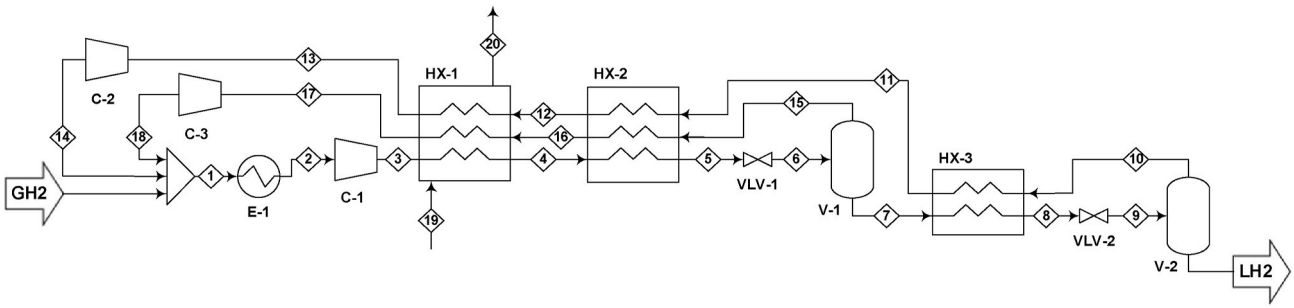

Fig. 2. Process scheme of LN_2 precooled Claude cycle for hydrogen liquefaction.

Table 6
Cooling duties, together with the corresponding utility, of the LN_2 precooled Claude cycle (Fig. 2).

Equipment	T_{IN} [°C]	T_{OUT} [°C]	Q [kW]	utility
E−1	165.4	40	7145.28	CW
C-1 intercooler(1)	143.9	40	5931.73	CW
C-1 intercooler(2)	144.3	25	6850.67	CW + RW

Table 7
Electric power consumptions of the LN_2 precooled Claude cycle (Fig. 2).

Equipment	P_{IN} [bar]	P_{OUT} [bar]	W [kW]
C-1	20	103	11933.18
C-2	1.3	20	956.03
C-3	5.5	20	7598.99

-216 °C and −240 °C at the output of TE-2 and TE-3, respectively. At the exit of the last heat exchanger HX-5, the processed hydrogen is expanded in J-T valve VLV-1 to a pressure of 1.3 bar for storage, reaching a temperature of −252 °C. Table 8 and Table 9 report the energy balance of the process in terms of cooling duties and electric power consumptions, respectively.

4.3. Mixed-refrigerant cascade process

The process diagram of the MR cascade process is taken from the article by Ansarinasab et al. [48]. This cascade liquefaction process consists of Joule-Brayton (J-B) cycles operating at different temperature levels. The refrigerant mixture for precooling consists of 17 mol% CH_4, 7 mol% C_2H_6, 18 mol% C_3H_8, 2 mol% n-C_4H_{10}, 15 mol% n-C_5H_{12}, 8 mol % R-14, 16 mol% C_2H_4, 16 mol% N_2, 1 mol% H_2, while the one for cooling is made of 83.61 mol% He, 10.20 mol% Ne and 6.19 mol% H_2.

Referring to the process scheme in Fig. 4, the hydrogen feed stream GH2 is precooled in the heat exchangers HX-1, HX-2 and HX-3 to −195 °C. After precooling, the processed hydrogen stream is cooled in the heat exchangers HX-4, HX-5 and HX-6 to −250 °C. Subsequently, the pressure is reduced to 1.3 bar in the J-T valve VLV-1 for storage. The

Table 8
Cooling duties, together with the corresponding utility, of the MR precooled Claude cycle (Fig. 3).

Equipment	T_{IN} [°C]	T_{OUT} [°C]	Q [kW]	utility
E−1	149.5	40	2184.33	CW
E−2	86.2	25	2110.04	CW + RW
E−3	264.8	40	1538.51	CW
E−4	273.3	25	10639.66	CW + RW

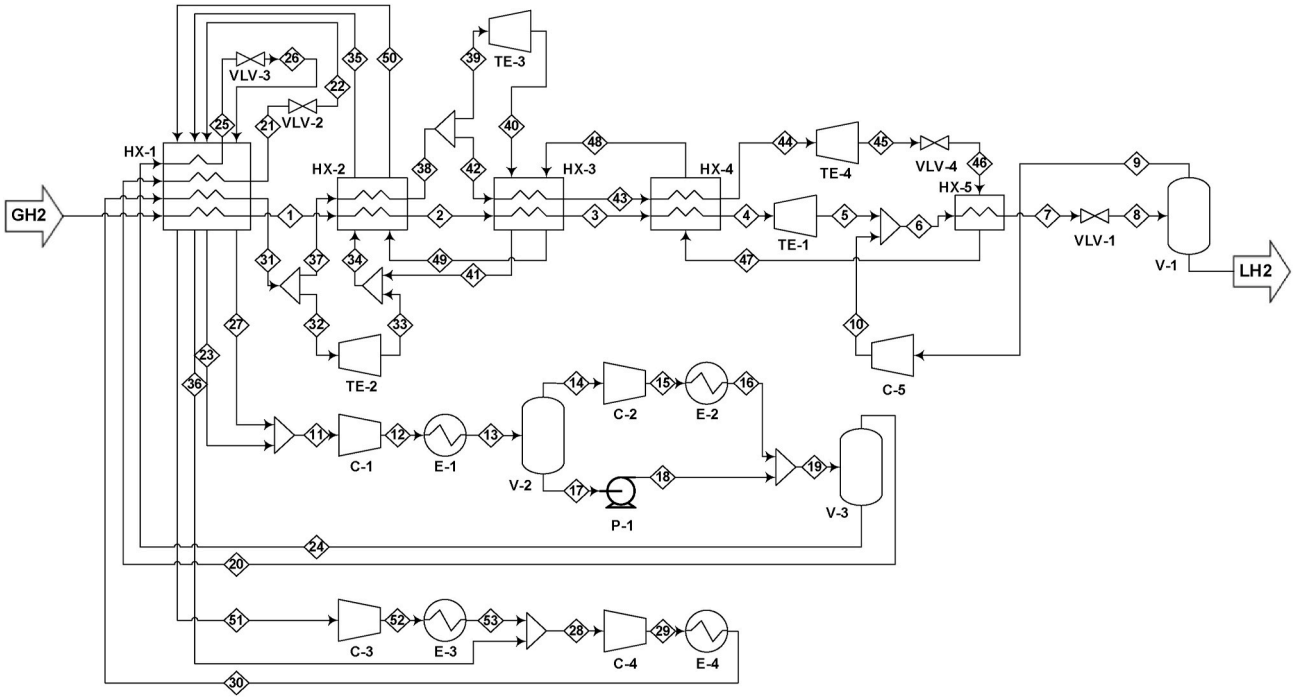

Fig. 3. Process scheme of MR precooled Claude cycle for hydrogen liquefaction.

Table 9
Electric power consumptions of the MR precooled Claude cycle (Fig. 3).

Equipment	P_{IN} [bar]	P_{OUT} [bar]	W [kW]
C-1	2.9	25	2094.50
C-2	25	50	543.00
C-3	1.4	8.3	1665.30
C-4	8.3	49.9	10661.55
C-5	1.3	5	4.72

precooling mixture (stream 11) is compressed to 16 bar in two compression stages, C-1 and C-2, with intercooling to 40 °C. The high-pressure stream 19 is separated into its phases in flash vessel V-3. The liquid (stream 33) is precooled to −34 °C in HX-1 and expanded to 2 bar in the turbine TE-3, to provide cooling in HX-1 at −39 °C. The vapor (stream 20) is precooled in HX-1 and separated into its liquid and vapor phases inside vessel V-4. After further precooling in HX-2, the liquid (stream 31) is expanded to 2 bar in the turbine TE-2, to provide cooling in HX-2 at −107 °C. The vapor (stream 22) is precooled in HX-2 and HX-3 and expanded in TE-1 so that the stream 25 enters the cold side of the HX-3 multi-pass exchanger at −199 °C to remove heat from the processed hydrogen. The cooling mixture (stream 36) is compressed to 10 bar in three compression stages, C-3, C-4 and C-5, with intercooling to 40 °C. The resulting stream is divided into three sub-streams which act as coolants in three J-B recuperative cycles operating at different temperature levels. In particular, the mixture reaches a temperature of −220, −240 and −250 °C at the outlet of TE-4, TE-5 and TE-6, respectively.

The cooling duties and electric power consumptions of the process are reported respectively in Table 10 and Table 11.

5. Simulation of the reconversion process

The reconversion from liquid to gaseous hydrogen consists in pumping, vaporization and, in case, compression. The process diagram of the regasification process is depicted in Fig. 5.

The pumping discharge pressure is chosen depending on the hydrogen destination after regasification. In case of hydrogen delivery to a H_2 valley the pressure is set to 30 bar, required to serve the industries in the neighborhoods of the valley. In case HRS are the end users of the delivered hydrogen, if centralized regasification is performed at the port of arrival, pumping to 320 bar is necessary to feed the tube trailers, operating at 250 bar, for compressed hydrogen distribution, while if decentralized regasification is carried out at the HRS, pumping to 900 bar is possible before vaporization, avoiding the need for downstream gas compression. For all the cases, it is assumed a pump efficiency of 0.6 [34] and CW as hot fluid in the vaporizer.

The energy balance of the regasification process for the different investigated cases is reported in Table 12.

In case of hydrogen delivery to HRS with centralized regasification at the port of arrival and compressed gaseous hydrogen distribution, compression to 900 bar at the refueling stations is required after tube trailer discharge. An efficiency of 0.65 is assumed for the refueling station compressors [34]. The compression process scheme is depicted in Fig. 6.

Table 13 presents the energy balance of the compression process.

6. Results and discussion

The block flow diagram (BFD), together with the detailed material balance throughout the entire value chain, is presented in Fig. 7a for the

Table 10
Cooling duties, together with the corresponding utility, of the MR cascade process (Fig. 4).

Equipment	T_{IN} [°C]	T_{OUT} [°C]	Q [kW]	utility
E−1	78.6	40	1023.47	CW
E−2	86.5	25	2928.76	CW + RW
E−3	185.9	40	4343.25	CW
E−4	178.6	40	4043.65	CW
E−5	161.7	40	3550.58	CW

Table 11
Electric power consumptions of the MR cascade process (Fig. 4).

Equipment	P_{IN} [bar]	P_{OUT} [bar]	W [kW]
C-1	2	7	1455.51
C-2	7	16	969.66
C-3	1	2.3	4373.99
C-4	2.3	5	4046.98
C-5	5	10	3556.79
C-6	1.3	20	19.86

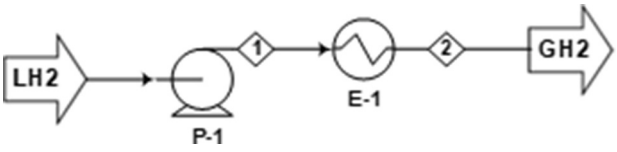

Fig. 5. Process scheme of liquefied hydrogen regasification.

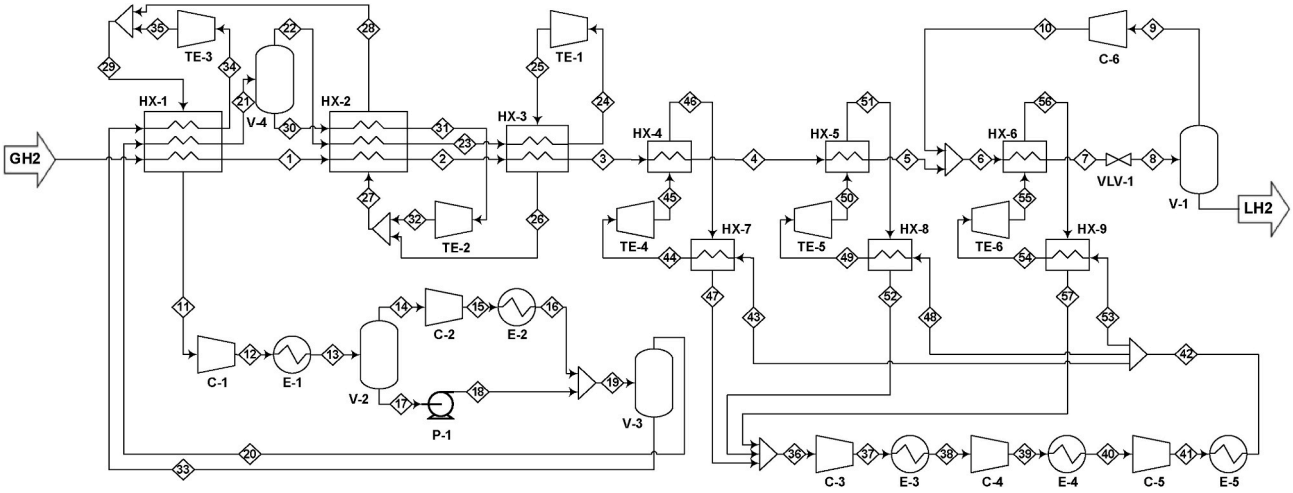

Fig. 4. Process scheme of MR cascade process for hydrogen liquefaction.

Table 12
Heating duty, provided by CW, and electric power consumption of the regasification process (Fig. 5).

Case	E−1			P-1		
	T_{IN} [°C]	T_{OUT} [°C]	Q [kW]	P_{IN} [bar]	P_{OUT} [bar]	W [kW]
H_2 valley	−247.9	20	2102.57	1.3	30	33.60
HRS centralized reconversion	−209.4	20	1842.00	1.3	320	373.06
HRS decentralized reconversion*	−145.9	20	16.17	1.3	900	12.42

case involving industrial end use of the delivered H_2, and in Fig. 7b for the case of H_2 utilization in the mobility sector, considering both centralized and decentralized regasification options.

In both cases of hydrogen delivery to a H_2 valley and to HRS, the hydrogen losses occur as boil off during sea transport. In case of H_2 destination to HRS approximately 86 stations can be served.

The economic evaluations performed on the liquefied hydrogen value chain are reported below, according to the methodology described in Section 3.

6.1. Conversion process

The investment and operating costs for the three considered liquefaction processes are evaluated based on the process simulations described in Section 4 and the results are summarized in Table 14.

As expected, the *CAPEX* increase with the process complexity, while the *OPEX* decrease. The computation of the levelized cost for the liquefaction step of the value chain allows to identify which process is the most cost-effective for the given basis of design. The MR precooled Claude cycle presents the best trade-off between investment and operating costs and, hence, it is the process selected in this case study to perform the liquefaction of hydrogen. In Fig. 8, the obtained results are juxtaposed with existing literature data in terms of *CAPEX*, categorized per process type. To facilitate meaningful comparisons across different estimations, the literature values are adjusted for H_2 liquefaction capacity using the six-tenths rule and for the base year using the *CEPCI*.

Fig. 8 enables to observe a significant variability in literature estimations concerning the LN_2 precooled Claude cycle. In particular, the value of Nexant [34] exhibits a substantial overestimation compared to the others. On the contrary, there is a good agreement among the estimations for the MR cascade process.

The *CAPEX* cost items of the preferred process are reported in Table 15, from which it is possible to notice that most of the investment costs are attributable to the compressors and heat exchangers.

The *OPEX*, detailed in Table 16, are equal to 101.31 M€/y and are mainly due to the cost of the electricity required to power the compressors.

The graph in Fig. 9 shows the extrapolation, obtained using the six-tenths rule, of the hydrogen liquefaction cost as a function of the plant's size for different values of the electricity cost. In particular, the solid green line corresponds to the "present" scenario (cost of electricity equal to 500 €/MWh), while the dashed green line represents the "future" scenario (cost of electricity equal to 220 €/MWh). The dots mark the costs corresponding to the size considered in this study on both curves. The cost of hydrogen liquefaction is significantly influenced by the electricity price, leading to a reduction of approximately 3 €/kg for liquefaction costs in the "future" scenario compared to the "present" one. The crosses denote the values of hydrogen liquefaction cost as found in the literature. Given the influence of the electricity price, the curves representing the calculated liquefaction cost as a function of the plant size for the different electricity cost values are plotted in the same color as the source for the respective electricity cost values. Specifically, the value of 100 €/MWh, used to plot the blue dashed line, is taken from Raab et al. [8] (liquefaction cost represented by a blue cross) and the value of 35 €/MWh, used to plot the violet dashed line, is sourced from Chodorowska and Farhadi [6] (liquefaction cost indicated by a violet cross). The report by Roland Berger [7] lacks information about the assumed electricity price. Looking at Fig. 9, a good agreement can be observed between the estimates obtained in this study and those from the existing literature.

6.2. Liquefied hydrogen transport, storage and distribution

The investment costs of sea transport are exclusively associated with the purchase of the vessel, having a capacity of 6700 m^3. On the contrary, the operating costs are associated with labor, fuel consumption, and CO_2 emissions. The obtained *CAPEX* and *OPEX* for the sea transport of LH_2 are respectively 57.81 M€ and 3.91 M€/y.

For the case involving hydrogen delivery to a H_2 valley, the procurement of 3 full-capacity storage tanks is required: one at the loading port, one at the unloading port and one at the H_2 valley. Each of these tanks has a capacity of 7300 m^3. The total *CAPEX* for this configuration amounts to 78.56 M€. For the case involving the transport of hydrogen to HRS, 2 full-capacity tanks are needed at the ports, resulting in *CAPEX* of 52.37 M€. Additionally, if regasification is performed at the HRS, a small-capacity tank for liquefied hydrogen is required to supply the process at every station, adding overall *CAPEX* of 7.53 M€.

For the cases of H_2 delivery to a H_2 valley and to HRS with regasification at the end users, the distribution of liquefied hydrogen necessitates the purchase of 6 trucks. The total *CAPEX* and *OPEX* are respectively 8.93 M€ and 1.59 M€/y. If, for the case of H_2 delivery to HRS, the regasification takes place at the unloading port, compressed gaseous hydrogen need to be distributed. This entails the purchase of 43 trucks, with overall *CAPEX* and *OPEX* of 37.64 M€ and 11.77 M€/y, respectively.

6.3. Reconversion process

In the case of hydrogen destination to a H_2 valley, the reconversion process includes pumping to 30 bar and vaporization, involving *CAPEX* of 0.81 M€ (Table 17) and *OPEX* of 2.11 M€/y (Table 18).

As regards the hydrogen delivery to HRS, the decentralized configuration involves pumping to 900 bar and vaporization at each of the 86

Table 13
Cooling duties, together with the corresponding utility, and electric power consumptions of the compression process (Fig. 6).

Equipment	T_{IN} [°C]	T_{OUT} [°C]	Q [kW]	utility
E−1	595.7	40	23.84	CW
E−2	601.62	40	24.70	CW
E−3	428.66	40	10.03	CW
Equipment	**P_{IN} [bar]**	**P_{OUT} [bar]**	**W [kW]**	
C-1	15	90	25.73	
C-2	90	450	26.03	
C-3	450	900	11.99	

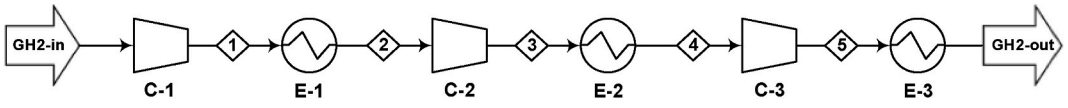

Fig. 6. Process scheme of gaseous hydrogen compression.

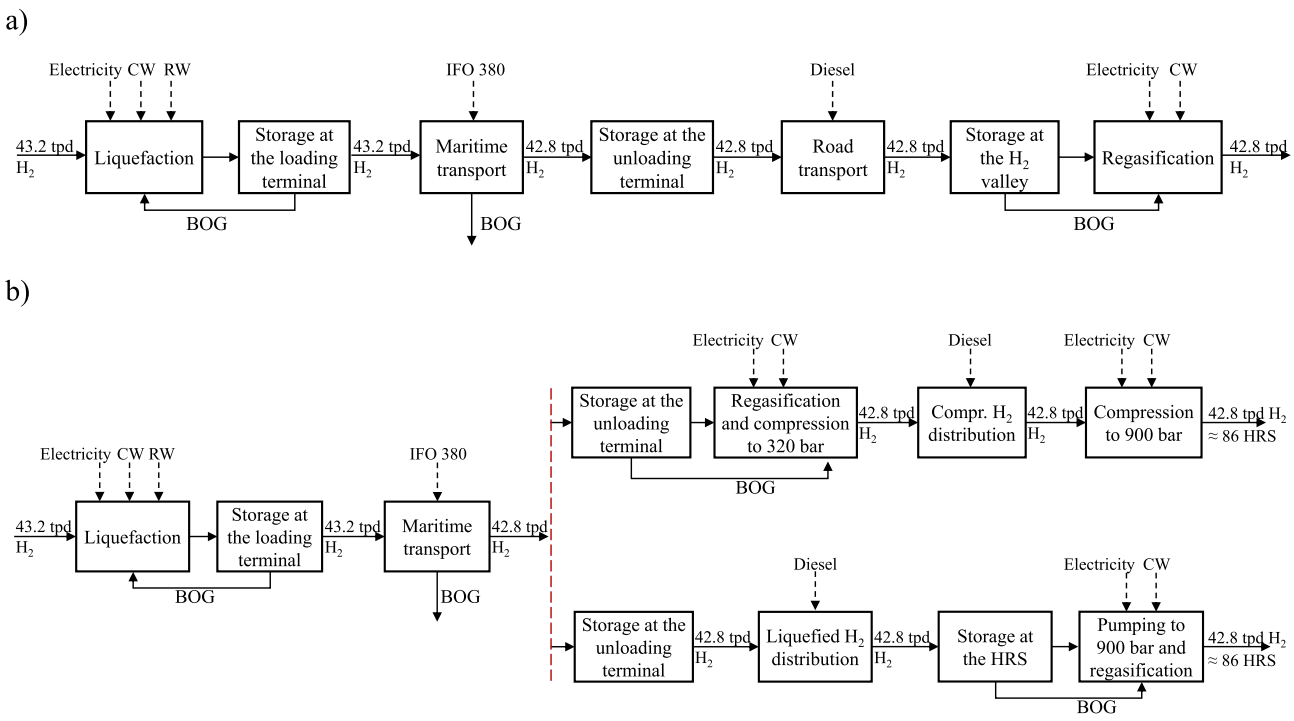

Fig. 7. BFD of the liquefied hydrogen value chain for the cases of H_2 destination to: a) a H_2 valley, b) HRS.

Table 14
CAPEX [M€], *OPEX* [M€/y] and *LCoHT* [€/kg] for the three considered hydrogen liquefaction processes.

	CAPEX [M€]	*OPEX* [M€/y]	*LCoHT* [€/kg]
LN_2 precooled Claude cycle	96.03	129.92	9.66
MR precooled Claude cycle	115.85	101.31	7.77
MR cascade process	138.77	101.12	7.89

served refueling stations with overall *CAPEX* and *OPEX* of 73.28 M€ and 69.55 M€/y, respectively. The costs incurred at the single refueling station are reported in Table 19, for the *CAPEX*, and in Table 20, for the *OPEX*.

The centralized alternative instead involves pumping to 320 bar and vaporization at the port of arrival, involving *CAPEX* of 2.08 M€ (Table 21) and *OPEX* of 4.14 M€/y (Table 22), and compression from the tube trailer discharge pressure to 900 bar at each refueling station, with overall *CAPEX* and *OPEX* of 106.98 M€ and 99.18 M€/y, respectively. The costs for compression incurred at the single refueling station are reported in Table 23, for the *CAPEX*, and in Table 24, for the *OPEX*.

6.4. Levelized Cost of Hydrogen Transport

The results in terms of *LCoHT* for each segment of the value chain are illustrated in Fig. 10 for the case of hydrogen utilization in the industrial sector and in Fig. 11 for the case of application to the mobility sector.

Regarding the application to the industrial sector, the total *LCoHT* is 9.16 €/kg in the "present" scenario, with a projected cost reduction to 6.14 €/kg in the "future" scenario. Analyzing Fig. 10, it becomes evident that the cost driver of the value chain is the liquefaction process, followed by storage and transport, while the impact of the regasification process on the overall *LCoHT* remains negligible. In the future, a reduction in the cost of hydrogen liquefaction is foreseen, attributable to the lower utility prices, particularly electricity, utilized in the process.

As regards the application to the mobility sector, the total *LCoHT* amounts to 14.20 €/kg and 17.71 €/kg when considering, respectively, the decentralized and centralized reconversion in the "present" scenario. In the future, these costs are projected to decrease to 10.96 €/kg and 13.49 €/kg, respectively. The cost reduction is more evident for the case

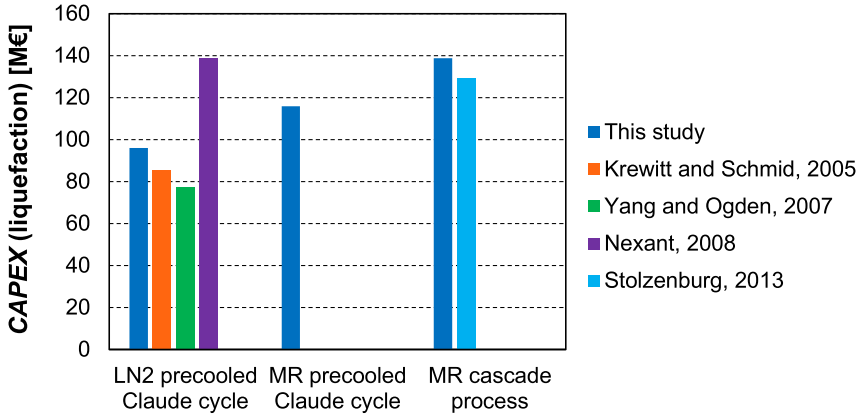

Fig. 8. *CAPEX* [M€] for the three considered hydrogen liquefaction processes: comparison between the results obtained in this study and the literature [34,49–51].

Table 15
CAPEX [M€] for the preferred liquefaction process. In the Figure the breakdown of the C_{BM}.

	Equipment	*Cost* [M€]
C_{BM}	Heat Exchangers	39.64
	Compressors	41.03
	Turbines	3.26
	Pumps	0.02
	Vertical Vessels	1.09
	Coldboxes	0.81
C_{TM}		101.32
CAPEX		115.85

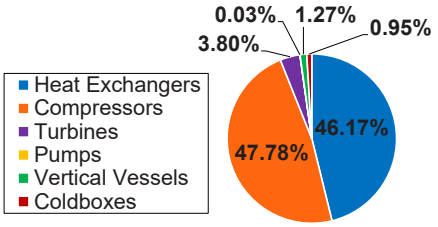

Table 16
OPEX [M€/y] for the preferred liquefaction process.

	Cost [M€/y]
C_{UT}	58.31
C_{OL}	0.80
other *DMC*	11.30
FMC	8.44
GE	22.46
OPEX	101.31

of centralized reconversion since the compression process strongly relies on electricity consumption, making it susceptible to fluctuations in utility prices. For the case of H_2 delivery to HRS, it is more economically advantageous to distribute liquefied hydrogen and carry out decentralized regasification at the refueling stations than performing centralized regasification at the unloading port and distributing compressed gaseous hydrogen, to be further compressed at the stations. Indeed, referring to Fig. 11, the higher cost related to building and operating multiple regasification processes at the HRS is still lower than the compressed hydrogen distribution, along with the additional compression costs to reach 900 bar.

7. Conclusions

The analysis conducted from a techno-economic perspective allowed for a detailed exploration of each step of the liquefied hydrogen value chain and provided insights into its potential implementation in the industrial and mobility sectors.

The first objective of the present article was to estimate the capital and operating expenditures of the cost-driving processes through simulation. This approach allows a meticulous evaluation of costs based on plant complexity and utility consumption, thus identifying the most cost-effective plant configuration for the given basis of design. Among the examined hydrogen liquefaction process configurations, the mixed refrigerant precooled Claude cycle presents the best trade-off between

Table 17
CAPEX [M€] for the regasification process in the case of hydrogen destination to a H_2 valley.

	Equipment	*Cost* [M€]
C_{BM}	Heat Exchangers	0.45
	Pumps	0.09
C_{TM}		0.64
CAPEX		0.81

Table 18
OPEX [M€/y] for the regasification process in the case of hydrogen destination to a H_2 valley.

	Cost [M€/y]
C_{UT}	0.16
C_{OL}	0.60
other *DMC*	0.32
FMC	0.48
GE	0.56
OPEX	2.11

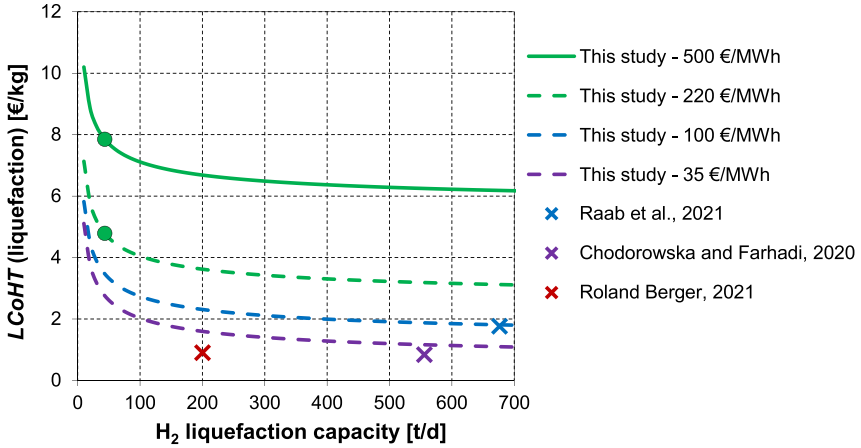

Fig. 9. *LCoHT* [€/kg] for the preferred hydrogen liquefaction process: comparison between the results obtained in this study and the literature [6–8].

Table 19
CAPEX [M€] for the regasification process in the case of hydrogen destination to HRS with decentralized configuration. Costs incurred at the single refueling station.

	Equipment	*Cost* [M€]
C_{BM}	Heat Exchangers	0.186
	Pumps	0.451
C_{TM}		0.752
CAPEX		0.856

Table 20
OPEX [M€/y] for the regasification process in the case of hydrogen destination to HRS with decentralized configuration. Costs incurred at the single refueling station.

	Cost [M€/y]
C_{UT}	0.050
C_{OL}	0.200
other *DMC*	0.150
FMC	0.200
GE	0.214
OPEX	0.813

Table 21
CAPEX [M€] for the regasification process in the case of hydrogen destination to a HRS with centralized configuration.

	Equipment	*Cost* [M€]
C_{BM}	Heat Exchangers	0.65
	Pumps	0.90
C_{TM}		1.83
CAPEX		2.08

Table 22
OPEX [M€/y] for the regasification process in the case of hydrogen destination to a HRS with centralized configuration.

	Cost [M€/y]
C_{UT}	1.51
C_{OL}	0.60
other *DMC*	0.47
FMC	0.57
GE	0.99
OPEX	4.14

Table 23
CAPEX [M€] for the compression process in the case of hydrogen destination to a HRS with centralized configuration. Costs incurred at the single refueling station.

	Equipment	*Cost* [M€]
C_{BM}	Heat Exchangers	0.428
	Compressors	0.487
C_{TM}		1.080
CAPEX		1.251

investment and operating costs for the medium plant size considered in this study.

The second objective was the assessment of the *LCoHT* based on the assumed end use of the delivered hydrogen, distinguishing between its application in the industrial sector (delivery to a H_2 valley) and mobility sector (delivery to Hydrogen Refueling Stations). The industrial sector application incurs the lowest costs as it eliminates the need to distribute to multiple end users and achieve high pressure levels. Among the

Table 24
OPEX [M€/y] for the compression process in the case of hydrogen destination to a HRS with centralized configuration. Costs incurred at the single refueling station.

	Cost [M€/y]
C_{UT}	0.256
C_{OL}	0.200
other *DMC*	0.187
FMC	0.227
GE	0.290
OPEX	1.159

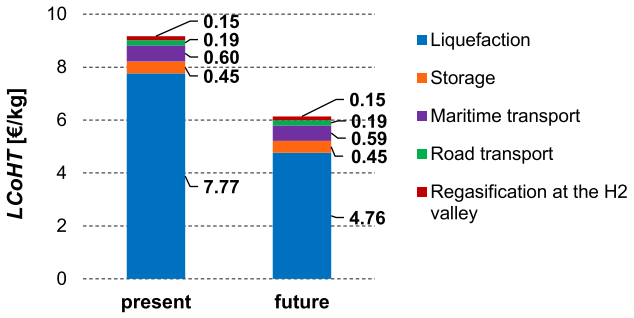

Fig. 10. *LCoHT* [€/kg] in the case of H_2 destination to a H_2 valley: comparison between the present and future scenarios.

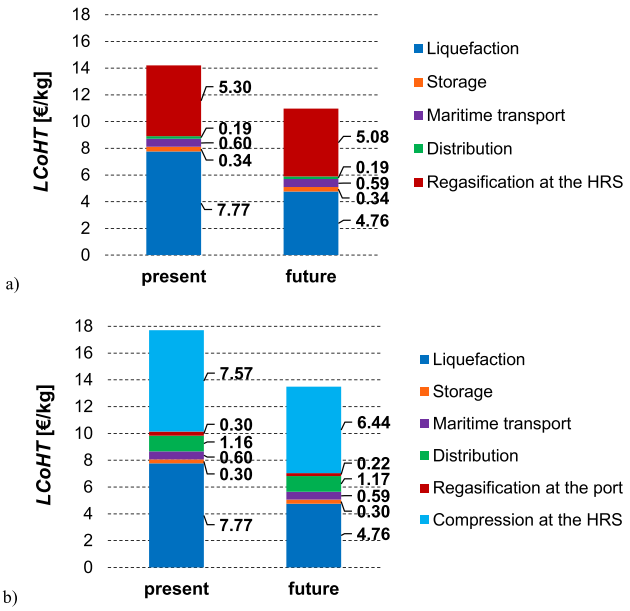

Fig. 11. *LCoHT* [€/kg] in the case of H_2 destination to HRS: comparison between the present and future scenarios when a) decentralized regasification takes place at the HRS and b) centralized regasification takes place at the port.

analyzed alternatives for hydrogen delivery to HRS, the most cost-effective one involves decentralized regasification at the refueling stations. It takes advantage from the lower mechanical power required to compress a liquid with respect to a gas. Also, this option is more environmentally friendly because fewer trucks are required for distribution, due to the higher hydrogen volumetric density, resulting in a lower fuel consumption. Moreover, liquefied hydrogen distribution entails lower safety issues with respect to compressed gaseous hydrogen: the lower storage pressure reduces the risk of tank rupture and explosion and the boil-off gas released at a slow rate is quickly dissipated and rises,

reducing the risk of accumulation and ignition.

In all the examined cases, the liquefaction process emerges as the cost driver. It is advisable to undertake additional research aimed at optimizing the process in order to reduce its costs.

This study represents a first step towards evaluating the viability of utilizing liquefied hydrogen as a means to transport low-cost African renewable energy to Europe. Future research should go through this study by implementing more rigorous plant layouts, with the aim of achieving a more precise economic estimation.

Declaration of competing interest

The authors declare that they have no known competing financial interests or personal relationships that could have appeared to influence the work reported in this paper.

References

[1] Restelli F, Spatolisano E, Pellegrini LA, De Angelis AR, Cattaneo S, Roccaro E. Detailed techno-economic assessment of ammonia as green H_2 carrier. Int J Hydrogen Energy 2023. https://doi.org/10.1016/j.ijhydene.2023.06.206.

[2] Schorn F, Breuer JL, Samsun RC, Schnorbus T, Heuser B, Peters R, Stolten D. Methanol as a renewable energy carrier: an assessment of production and transportation costs for selected global locations. Adv Appl Energy 2021;3:100050.

[3] Spatolisano E, Restelli F, Matichecchia A, Pellegrini LA, De Angelis AR, Cattaneo S, et al. Assessing opportunities and weaknesses of green hydrogen transport via LOHC through a detailed techno-economic analysis. Int J Hydrogen Energy 2023. https://doi.org/10.1016/j.ijhydene.2023.08.040.

[4] Teichmann D, Arlt W, Wasserscheid P. Liquid Organic Hydrogen Carriers as an efficient vector for the transport and storage of renewable energy. Int J Hydrogen Energy 2012;37:18118–32.

[5] Okunlola A, Giwa T, Di Lullo G, Davis M, Gemechu E, Kumar A. Techno-economic assessment of low-carbon hydrogen export from western Canada to eastern Canada, the USA, the Asia-Pacific, and Europe. Int J Hydrogen Energy 2022;47:6453–77.

[6] Chodorowska N, Farhadi M. H_2 value chain comparing different transport vectors. GPA Europe Virtual Conference. 2021.

[7] Berger R. Hydrogen transportation. 2021.

[8] Raab M, Maier S, Dietrich R-U. Comparative techno-economic assessment of a large-scale hydrogen transport via liquid transport media. Int J Hydrogen Energy 2021;46:11956–68.

[9] Gallardo FI, Ferrario AM, Lamagna M, Bocci E, Garcia DA, Baeza-Jeria TE. A Techno-Economic Analysis of solar hydrogen production by electrolysis in the north of Chile and the case of exportation from Atacama Desert to Japan. Int J Hydrogen Energy 2021;46:13709–28.

[10] Song S, Lin H, Sherman P, Yang X, Nielsen CP, Chen X, McElroy MB. Production of hydrogen from offshore wind in China and cost-competitive supply to Japan. Nat Commun 2021;12:6953.

[11] Niermann M, Timmerberg S, Drünert S, Kaltschmitt M. Liquid Organic Hydrogen Carriers and alternatives for international transport of renewable hydrogen. Renew Sustain Energy Rev 2021;135:110171.

[12] Hong X, Thaore VB, Karimi IA, Farooq S, Wang X, Usadi AK, et al. Techno-enviro-economic analyses of hydrogen supply chains with an ASEAN case study. Int J Hydrogen Energy 2021;46:32914–28.

[13] Ishimoto Y, Voldsund M, Nekså P, Roussanaly S, Berstad D, Gardarsdottir SO. Large-scale production and transport of hydrogen from Norway to Europe and Japan: value chain analysis and comparison of liquid hydrogen and ammonia as energy carriers. Int J Hydrogen Energy 2020;45:32865–83.

[14] Hank C, Sternberg A, Köppel N, Holst M, Smolinka T, Schaadt A, et al. Energy efficiency and economic assessment of imported energy carriers based on renewable electricity. Sustain Energy Fuels 2020;4:2256–73.

[15] Hydrogen Import Coalition. Shipping sun and wind to Belgium is key in climate neutral economy. Technology 2021;14:19.

[16] Wijayanta AT, Oda T, Purnomo CW, Kashiwagi T, Aziz M. Liquid hydrogen, methylcyclohexane, and ammonia as potential hydrogen storage: comparison review. Int J Hydrogen Energy 2019;44:15026–44.

[17] IEA. The future of hydrogen. 2019.

[18] Kamiya S, Nishimura M, Harada E. Study on introduction of CO2 free energy to Japan with liquid hydrogen. Phys Procedia 2015;67:11–9.

[19] Watanabe T, Murata K, Kamiya S, Ota KI. Cost estimation of transported hydrogen, produced by overseas wind power generations. 18th World Hydrogen Energy Conference. Forschung Jülich GmbH Zentralbiblio Essen 2010:547–57.

[20] Stiller C, Svensson AM, Møller-Holst S, Bünger U, Espegren KA, Holm ØB, et al. Options for CO_2-lean hydrogen export from Norway to Germany. Energy 2008;33:1623–33.

[21] Wietschel M, Hasenauer U. Feasibility of hydrogen corridors between the EU and its neighbouring countries. Renew Energy 2007;32:2129–46.

[22] Shah SFA, Khan IA, Khan HA. Performance evaluation of two similar 100MW solar PV plants located in environmentally homogeneous conditions. IEEE Access 2019;7:161697–707.

[23] Chance C. Focus on hydrogen: Japan's energy strategy for hydrogen and ammonia. 2022. https://www.cliffordchance.com/content/dam/cliffordchance/briefings/2022/08/focus-on-hydrogen-in-japan.pdf. [Accessed 24 March 2023].

[24] AspenTech. Aspen Plus®. Burlington (MA), United States: AspenTech; 2019.

[25] Martin J, Neumann A, Ødegård A. Sustainable hydrogen fuels versus fossil fuels for trucking, shipping and aviation: a dynamic cost model. MIT Center for Energy and Environmental Policy Research; 2022.

[26] Lorenczik S, Kim S, Wanner B, Bermudez Menendez JM, Remme U, Hasegawa T, et al. Projected costs of generating electricity-2020 edition. Organisation for Economic Co-Operation and Development; 2020.

[27] European Central Bank. Euro foreign exchange reference rates. https://www.ecb.europa.eu/stats/policy_and_exchange_rates/euro_reference_exchange_rates/html/eurofxref-graph-usd.en.html. [Accessed 24 March 2023].

[28] Turton R, Bailie RC, Whiting WB, Shaeiwitz JA. Analysis, synthesis and design of chemical processes. Pearson Education; 2008.

[29] Guthrie KM. Capital cost estimating. Chem Eng 1969;76:114.

[30] Rogers H. LNG Shipping Forecast: costs rebounding, outlook uncertain. 2018.

[31] Fikri M, Hendrarsakti J, Sambodho K, Felayati F, Octaviani N, Giranza M, et al. Estimating capital cost of small scale LNG carrier. In: Proceedings of the 3rd International Conference on Marine Technology. Surabaya, Indonesia: SENTA; 2019. p. 5–6.

[32] Damen. https://products.damen.com/-/media/products/images/clusters-groups/shipping/liquefied-gas-carrier/liquefied-gas-carrier-7500-lng/downloads/product_sheet_damen_liquefied_gas_carrier_7500_lng_10_2017.pdf?rev=7e8230a833e1458ca06c29a4b7a6b5e4. [Accessed 24 January 2023].

[33] EIA. Carbon dioxide emissions coefficients. 2022. https://www.eia.gov/environment/emissions/co2_vol_mass.php. [Accessed 24 March 2023].

[34] Nexant Inc., Air Liquide, Argonne National Laboratory, Chevron Technology Venture, Gas Technology Institute, National Renewable Energy Laboratory. H2A hydrogen delivery infrastructure analysis models and conventional pathway options analysis results. 2008.

[35] Simbeck D, Chang E. Hydrogen supply: cost estimate for hydrogen pathways–scoping analysis, vol. 71. National Renewable Energy Laboratory; 2002.

[36] DOE. Multi-year research, development and demonstration plan - 3.2 hydrogen delivery. 2015.

[37] Reuß M, Grube T, Robinius M, Preuster P, Wasserscheid P, Stolten D. Seasonal storage and alternative carriers: a flexible hydrogen supply chain model. Appl Energy 2017;200:290–302.

[38] Zhang T, Uratani J, Huang Y, Xu L, Griffiths S, Ding Y. Hydrogen liquefaction and storage: recent progress and perspectives. Renew Sustain Energy Rev 2023;176:113204.

[39] Al Ghafri SZS, Munro S, Cardella U, Funke T, Notardonato W, Trusler JPM, et al. Hydrogen liquefaction: a review of the fundamental physics, engineering practice and future opportunities. Energy Environ Sci 2022;15:2690–731.

[40] Yin L, Ju Y. Review on the design and optimization of hydrogen liquefaction processes. Front Energy 2020;14:530–44.

[41] Aasadnia M, Mehrpooya M. Large-scale liquid hydrogen production methods and approaches: a review. Appl Energy 2018;212:57–83.

[42] Restelli F, Spatolisano E, Pellegrini LA. Hydrogen liquefaction: a systematic approach to its thermodynamic modeling. Chem Eng Transac 2023;99:433–8.

[43] Leachman JW, Jacobsen RT, Penoncello SG, Lemmon EW. Fundamental equations of state for parahydrogen, normal hydrogen, and orthohydrogen. J Phys Chem Ref Data 2009;38:721–48.

[44] Valenti G, Macchi E, Brioschi S. The influence of the thermodynamic model of equilibrium-hydrogen on the simulation of its liquefaction. Int J Hydrogen Energy 2012;37:10779–88.

[45] Balasubramanian R, Abishek A, Gobinath S, Jaivignesh K. Alternative fuel: hydrogen and its thermodynamic behaviour. J Human Earth Future 2022;3:195–203.

[46] Crawford DB. Hydrogen liquefaction and conversion systems. Google Patents; 1963.

[47] Cardella U, Decker L, Sundberg J, Klein H. Process optimization for large-scale hydrogen liquefaction. Int J Hydrogen Energy 2017;42:12339–54.

[48] Ansarinasab H, Mehrpooya M, Sadeghzadeh M. An exergy-based investigation on hydrogen liquefaction plant-exergy, exergoeconomic, and exergoenvironmental analyses. J Clean Prod 2019;210:530–41.

[49] Krewitt W, Schmid S. WP 1.5 common information database D 1.1 fuel cell technologies and hydrogen production/distribution options. 2005.

[50] Yang C, Ogden J. Determining the lowest-cost hydrogen delivery mode. Int J Hydrogen Energy 2007;32:268–86.

[51] Stolzenburg K, Mubbala R. Hydrogen liquefaction report. Integrated design for demonstration of efficient liquefaction of hydrogen (IDEALHY). FCH JU; 2013.